Origin of backstreaming electrons within the quasi-perpendicular foreshock region: Two-dimensional self-consistent PIC simulation

Philippe Savoini, Bertrand Lembège, J. Stienlet

Origin of backstreaming electrons within the quasi-perpendicular foreshock region: Two-dimensional self-consistent PIC simulation

P. Savoini,[1] B. Lembége,[2] and J. Stienlet[1]

Received 7 January 2010; revised 6 March 2010; accepted 19 April 2010; published 14 September 2010.

[1] The foreshock region is populated by energetic backstreaming particles (electrons and ions) issued from the shock after having interacted with it. Several aspects concerning the origin of these high-energy particles and their corresponding acceleration mechanisms are still unresolved. The present study is focused on a quasi-perpendicular curved shock and associated electron foreshock region (i.e., for $90° \geq \theta_{Bn} \geq 45°$, where θ_{Bn} is the angle between the shock normal and the upstream magnetostatic field). Two-dimensional full-particle simulation is used in order to include self-consistently the electron and ion dynamics, the full dynamics of the shock, the curvature effects and the time-of-flight effects. All expected salient features of the bow shock are recovered both for particles and for electromagnetic fields. Present simulations evidence that the fast-Fermi acceleration (magnetic mirror) mechanism, which is commonly accepted, is certainly not the unique process responsible for the formation of energetic backstreaming electrons. Other mechanisms also contribute. More precisely, three different classes of backstreaming electrons are identified according to their individual penetration depth within the shock front: (i) "magnetic mirrored" electrons which only suffer a specular reflection at the front, (ii) "trapped" electrons which succeed to penetrate the overshoot region and suffer a local trapping within the parallel electrostatic potential at the overshoot, and (iii) "leaked" electrons which penetrate even much deeper into the downstream region. "Trapped" and "leaked" electrons succeed to find appropriate conditions to escape from the shock and to be reinjected back upstream. All these different types of electrons contribute together to the formation of energetic field-aligned beam. The acceleration mechanisms associated to each electron class and/or escape conditions are analyzed and discussed.

Citation: Savoini, P., B. Lembége, and J. Stienlet (2010), Origin of backstreaming electrons within the quasi-perpendicular foreshock region: Two-dimensional self-consistent PIC simulation, *J. Geophys. Res.*, *115*, A09104, doi:10.1029/2010JA015263.

1. Introduction

[2] Experimental observations have evidenced the foreshock as the upstream region defined between the curved terrestrial bow shock and the magnetic field line tangent to the bow shock around $\theta_{Bn} = 90°$. This region is populated by energetic particles (electrons and ions) backstreaming from the shock and associated with wave activity. Since the early 1970s, the foreshock has been extensively studied experimentally [*Filbert and Kellogg*, 1979; *Anderson et al.*, 1979; *Anderson*, 1981; *Feldman et al.*, 1983; *Fitzenreiter et al.*, 1996; *Bosqued et al.*, 1996; *Yin et al.*, 1998; *Kasaba et al.*, 1977].

[3] In this paper, we will focus our attention mainly on the electron foreshock but take into account the full ion dynamics as well. The fast-Fermi-type (also named magnetic mirror) mechanism has been proposed theoretically in order to account for the formation of energetic reflected electrons [*Leroy and Mangeney*, 1984; *Wu*, 1984; *Cairns*, 1987; *Krauss-Varban and Wu*, 1989; *Fitzenreiter et al.*, 1990]. In short, for oblique shock, a part of the incoming electrons (in particular those having a large perpendicular velocity component) cannot overcome the barrier represented by the strong gradients of the macroscopic E and B fields at the ramp and are reflected upstream. These features lead to the following consequences: (i) a typical magnetic mirrored electron suffers a specular-type reflection, has a very short interaction time with the shock front, and gets only a parallel energy gain during this reflection; (ii) these reflected electrons are characterized by a loss cone distribution function; (iii) as the angle θ_{Bn} approaches 90°, the electron energy gain increases but the number of reflected electrons decreases; for $\theta_{Bn} = 90°$ all incoming electrons are directly transmitted and no electron is reflected; (iv) although the reflection process is mainly dictated by the magnetic field, the electrostatic field contributes in the sense that it widens the loss cone distribution. Although this picture has been confirmed by a self-consistent approach based on the use of 2-D full-particle simulation of a curved shock, it is shown to be oversimplified in the sense that other mechanisms also contribute to the electrons reflection [*Savoini and Lembège*, 2001]. Such simulations include

[1]LPP, UPMC, Palaiseau, France.
[2]LATMOS-IPSL-UVSQ, Guyancourt, France.

0148-0227/10/2010JA015263

Table 1. Upstream Numerical Parameters

Parameters	Electrons	Ions
$\widetilde{v}_{th}$	0.3	0.04
$\widetilde{\lambda}_D$	0.42	0.34
$\widetilde{\rho}_c$	0.84	28
$\widetilde{c}/\widetilde{\omega}_p$	3	19
$\widetilde{\omega}_c$	0.5	0.012
$\widetilde{\omega}_p$	1	0.155
$\widetilde{\tau}_c$	13	524
$\widetilde{\beta}$	0.16	0.10
$\widetilde{V}_A$	0.23	0.23

full kinetic effects of both particle species, the full dynamics of the shock front, and its curvature effects, in addition to the inhomogeneity and nonstationary effects of the shock front. These self-consistent simulations were also able to reproduce the "bump-in-tail" electron distribution function in the foreshock region in good agreement with experimental observations [*Klimas and Fitzenreiter*, 1988; *Fitzenreiter et al.*, 1990; *Fitzenreiter*, 1995]. By analyzing these local distribution functions, *Savoini and Lembège* [2001] have shown that backstreaming electrons are composed with two populations: (i) a low parallel energy population characterized by a loss cone distribution in perpendicular distribution (electron ring) which corresponds to magnetic mirrored electrons and (ii) a high parallel energy population corresponding to field aligned beam but not associated to the magnetic mirror mechanism. However, these simulations raised several main questions that have not yet been resolved: What are the basic mechanisms responsible for the second population? Does there exist other backstreaming populations (for example, the "leaked" electrons which correspond to those which succeed to penetrate within the downstream region before escaping into the upstream region). Why has this population not been observed in these simulations? Do they really exist? If yes, why have they not been noted? The purpose of the present paper is to answer these questions by analyzing the time trajectories of the backstreaming electrons using a self-consistent approach.

[4] The paper is organized as follows. Simulation conditions and the method for generating the bow shock are summarized in section 2. Section 3 presents numerical results obtained for the main characteristic field components of the curved shock and for the electron time trajectory analysis. Finally, concluding remarks are given in section 4.

2. Numerical Conditions

[5] Present simulations have been performed with a 2.5-dimensional, fully electromagnetic, relativistic particle code using standard finite-size particle techniques. Details have been given by *Lembège and Savoini* [1992] and *Savoini and Lembège* [1994]. For a description of the self-consistent curved shock front see *Savoini and Lembège* [2001]. In short, nonperiodic conditions are applied along the x direction ($\widetilde{L}_x = 95\widetilde{c}/\widetilde{\omega}_{pi}$) within the simulation box and periodic conditions are used along y direction ($\widetilde{L}_y = 110\widetilde{c}/\widetilde{\omega}_{pi}$). All quantities with "~" are in normalized units. One important point concerns the orientation of the magnetostatic field $\vec{B}_{to}$ which is partially lying outside the simulation plane. Subscripts "l" and "t" are used respectively for defining the longitudinal and transverse components of the fields. The curvature (rough half circle) of the generated shock front allows herein a continuous variation of θ_{Bn} from 90° to 45° simulating the whole quasi-perpendicular domain of shock propagation. Such a configuration provides the accessibility for the electrons to flow along the magnetic field lines outside the simulation plane and to have a moderate projected displacement within the X-Y plane. Note that this angular range is larger than that used in the previous simulation ($90° \geq \theta_{Bn} \geq 65°$) of *Savoini and Lembège* [2001].

[6] The radius of the magnetic cylinder (used as a magnetic piston to generate the shock) has been chosen carefully so, after a short transient period $\widetilde{t} \leq 0.2\widetilde{\tau}_{ci}$, the curvature radius $\widetilde{R}_c$ of the shock is much larger than the upstream ion Larmor radius ($\widetilde{R}_c \geq 34\widetilde{\rho}_{ci}$, i.e., $\approx 200\widetilde{\rho}_{ce}$); $\widetilde{\tau}_{ci}$ is the upstream ion gyroperiod.

[7] Sizes of the simulation box and time of the run are large enough to cover all characteristic space and timescales for both particle species ($\widetilde{t}_{\text{simul}} = 2.2\widetilde{\tau}_{ci,us}$ where $\widetilde{\tau}_{\text{ci,us}}$ is the upstream ion gyroperiod), and so dynamics of the shock is independent of initial conditions. At the present stage of the study, it is important to point out that only the electron foreshock is investigated. The analysis of the ion foreshock is beyond the scope of the paper.

[8] Initial plasma conditions are summarized as follows: light velocity $\widetilde{c} = 3$ and temperature ratio between ion and electron population $T_e/T_i = 1.58$. A mass ratio $m_i/m_e = 42$ is used in order to save CPU time and the Alfvèn velocity $\widetilde{v}_A = 0.23$. The shock is in supercritical regime; as a reference, the Alfvèn Mach number measured at $\theta_{Bn} = 90°$ is $M_A = v_{\text{shock}}/v_A = 3$ and slightly varies with a decreasing θ_{Bn}. All electrons and ions parameters are summarized in Table 1. The curvature radius of the shock reached at the end time of the simulation is 660 ρ_{ci}, where ρ_{ci} is the upstream ion gyroradius.

3. Numerical Results

[9] Before analyzing the backstreaming electrons populating the foreshock region, we will focus on the salient features of the electromagnetic fields of the curved shock front itself and its time evolution, since these have a key impact on the electron dynamics.

3.1. Electric and Magnetic Fields

[10] An enlarged view of the magnetic field z component B_{tz} in the X-Y simulation plane is plotted at late time of the simulation $\widetilde{t} = 2.2\widetilde{\tau}_{ci}$ in Figure 1a. The curved shock is localized at the external edge of the half-disk observed in this picture. It is the first time to our knowledge that the whole quasi-perpendicular domain ($90° \geq \theta_{Bn} \geq 45°$) has been obtained self-consistently with a full particle code. This represents an extension of our previous work [*Savoini and Lembège*, 2001]. In short, the magnetic field profile continuously evolves from a well-defined steplike pattern (characterized by a narrow thickness of the front) for $\theta_{Bn} = 90°$, to a much wider and more turbulent profile as θ_{Bn} decreases. A comparison with ion phase space (not shown here) confirms that the observed foot is well related to a noticeable number of reflected ions and that their accumulation is responsible for the cyclic reformation of the shock front. This self-reformation has been already observed for

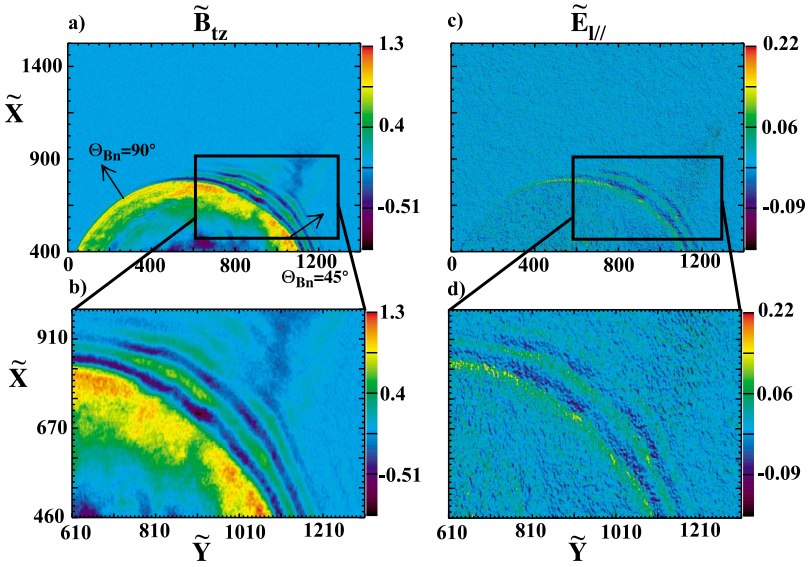

Figure 1. Enlarged view of the simulation plane X-Y plotted at time $\widetilde{t} = 2.2\widetilde{\tau}_{ci}$, where $\widetilde{\tau}_{ci}$ is the upstream cyclotronic ion period showing the developed curved shock. (a and b) The main magnetic field component B_{tz}; (c and d) the local self-consistent parallel electrostatic field $E_{l||}$ (above view). The magnetostatic field B_{to} is lying partially outside the simulation plane such that the whole angular range of curved shock is lying within $90° \geq \theta_{Bn} \geq 45°$. For reference, straight arrows plotted in Figure 1a represent the normal of the shock front at $\theta_{Bn} = 90°$ and $\theta_{Bn} = 45°$.

planar quasi-perpendicular shocks in 1-D [*Lembège and Dawson*, 1987] and 2-D [*Lembège and Savoini*, 1992] full-particle simulations and disappears for large deviation of θ_{Bn} (i.e., herein for $\theta_{Bn} \leq 72°$).

[11] In addition, a whistler precursor is emitted into the upstream region from the shock front for larger deviation angle $\theta_{Bn} \leq 60°$. Such electromagnetic precursor has been already observed for oblique planar shock wave, respectively, in 1-D [*Liewer et al.*, 1991] and 2-D PIC simulations [*Lembège and Savoini*, 1992]. In agreement with the dispersion relation [e.g., *Tidman and Krall*, 1971; *Mellott*, 1985], the dispersion effects become strong and an electromagnetic precursor is emitted with a decreasing wavelength (and amplitude). Throughout the run, the precursor wave train continued to extend upstream farther from the shock front until it disappears into the upstream electromagnetic turbulence. The identification and analysis of the upstream turbulence is beyond the scope of this paper but such wave activity seems well correlated with the interaction of the backstreaming electrons and the solar wind. Nevertheless, the wave crests nearer the shock front have reached steady-state amplitudes, and these have a velocity comparable to that of the shock front ($V_\phi = V_{\rm shock}$). Then, the linear dispersion relation gives a wavelength $\lambda_w = 38(27)$ for the standing precursor as $\theta_{Bn} \approx 45°$ (60°) to compare with the wavelengths $\lambda_w \approx 33$ (30) observed in our simulation. We obtain a relative good quantitative agreement. The progressive decay of the precursor with distance from the shock front indicates the presence of some damping mechanisms as in work by *Liewer et al.* [1991].

[12] The inclusion of the full shock curvature allows us to observe the competition between the increasing wave numbers (as θ_{Bn} decreases) and the Landau damping (mainly dependent of the ratio $v_{\phi||}/v_{\rm the}$, where $v_{\phi||}$ is the parallel phase velocity of the precursor and $v_{\rm the}$ the electron thermal velocity). Indeed, as the precursor propagates away front the shock front for $\theta_{Bn} \leq 60°$, its parallel phase velocity falls further inside the electron distribution for decreasing θ_{Bn} and more damping is expected. One can then observe the whole continuous transition from relatively weak nonlinear Landau damping ($v_{\phi||}/v_{\rm the} \approx 5.6$ and 2.8 for $\theta_{Bn} \approx 80°$ and 60° respectively) to linear Landau damping ($v_{\phi||}/v_{\rm the} \approx 1.6$ as θ_{Bn} decreases to 45°). Different processes then take place simultaneously as θ_{Bn} decreases from the critical angle below which the whistler precursor is emitted: the whistler precursor amplitude increases while the Landau damping varies from nonlinear to linear which balances the nonlinear steepening of the shock front. As a consequence, for very large angular deviations ($\theta_{Bn} \leq 55°$), present results show that the amplitude of the shock front decreases locally to low values (i.e., by a factor of 2 for $\theta_{Bn} \approx 53°$), reducing its magnetic/electric barrier in proportion.

[13] Indeed, the electrostatic field is maximum at the ramp of the curved shock (space charge effects). This component is known to accelerate the "incoming" solar wind electrons to the downstream region (we are in the "solar wind" reference frame). The electrostatic field $\widetilde{E}_l$ then lies along the shock normal and acts as an electrostatic barrier for the transmitted electrons which have to overcome it when escaping into the upstream region ("leaked" electrons). Figures 1c and 1d show a 2-D map of its parallel component $\widetilde{E}_{l||}$ in the same format as the magnetic field. Obviously, for the perpendicular direction ($\theta_{Bn} \approx 90°$), no parallel electrostatic field is observed and it begins to increase as θ_{Bn} decreases. As evidenced in Figure 1d, the drastic local decrease of the magnetic field amplitude around $\theta_{Bn} = 50°$ is accompanied by a similar behavior in the electrostatic field (and its $\widetilde{E}_{l||}$ component). This creates a certain local

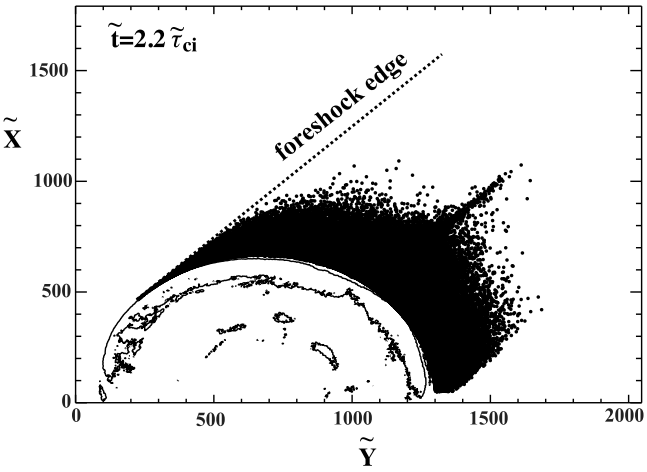

Figure 2. Locations of foreshock electrons within the simulation plane at the end of the simulation time $\tilde{t} = 2.2\tilde{\tau}_{ci}$ satisfying the criteria detailed in the text. The foreshock edge fits quite well the projected magnetic field line tangent to the curved front (thick dotted line).

"*permeability*" of the shock front, and some downstream electrons should have much less difficulty passing through the barrier and escaping into the upstream region.

[14] It is important to point out that even a relatively small value of the parallel electric field (maximum $E_{l\|} \approx 0.22$ in Figure 1) strongly affects the light population (i.e., electrons) which can stream freely along the magnetic field. The impact of the parallel electric field component has been already studied both experimentally [*Walker et al.*, 2004; *Bale and Mozer*, 2007; *Lefebvre et al.*, 2007] and numerically with self-consistent simulations of planar shocks [*Savoini and Lembège*, 1994; *Lembège and Savoini*, 2002] but never in the context of a self-consistent foreshock. Then, we will investigate how this component can modify the dynamic of the backstreaming electrons.

3.2. Electron Dynamics

[15] The procedure used for identifying the backstreaming electrons in the foreshock region in our 2-D simulations is based on three selection criteria: (i) electrons have to be in the upstream region at the end of the run; (ii) they must have interacted with the shock front (whatever the interaction type is); and finally, and more importantly, (iii) during their interaction, they have gained enough energy to be differentiated from background ambient electrons (herein, we choosed an energy gain $E_{\rm end}/E_{\rm init} \geq 2$). The advantage of the present method is to eliminate safely electrons which do not have high contrast with respect to the background solar wind distribution without any *a priori* idea on the energization processes of the selected electrons, neither on their original upstream location.

[16] The selected backstreaming electrons are plotted in the X-Y simulation plane in Figure 2 and represent ≈4.7% of all electrons interacting with the shock wave (i.e., roughly 95.3% of incoming electrons are directly transmitted). This value represents a lower estimate of the real percentage of foreshock electrons since some of these have been certainly eliminated by the selection criteria used herein. The selected particles populate the whole foreshock region and their spatial extension is clearly limited by the magnetic field line tangent to the shock front (edge of the foreshock). Such a behavior had not been so clearly observed in the previous study [*Savoini and Lembège*, 2001] mainly because of the smaller time length of the run which restricted the spatial extension of the electron foreshock.

[17] These present results are in very good agreement with the well-known characteristic of the Earth's bow shock [*Fitzenreiter et al.*, 1990; *Onsager and Thomsen*, 1991; *Yin et al.*, 1998; *Fitzenreiter*, 1995, and references therein]. Moreover, we observe local distribution functions which exhibit the *bump-on-tail* feature whose origin not only is due to the magnetic mirror (fast Fermi) reflection but also requires other energization processes as evidenced by *Savoini and Lembège* [2001]. A possible other mechanism was described by *Lembège and Savoini* [2002] for 2-D planar shock wave (including the front rippling) but this study was limited to one particular propagation angle $\theta_{Bn} = 55°$. On the other hand, a main experimental difficulty consists in measuring directly the DC electric field scale at the shock front because of fluctuations in the electric potential, even if some important results have been obtained recently [*Lefebvre et al.*, 2007]. In contrast with experimental observations, full particle simulations, where all scales are determined self-consistently and are more easily accessible, are appropriate for such a study. In particular, these allow us to identify herein the different acceleration mechanisms by analyzing carefully the time trajectories of the selected backstreaming electrons.

[18] It is important to point out that such electrons are not test particles based on fixed (precomputed) electromagnetic fields. We choose a sampling of 1500 particles (among the backstreaming electrons) to cover a large spectrum of final kinetic energy. The considered number of these sampled electrons has been reduced in order to focus only on all significant physical quantities seen by the particles every $0.2\tau_{ce}$. Obviously, this sampling is not large enough to allow statistical studies on the foreshock energy partition. Nevertheless, this sampling is large enough to identify clearly three different classes of backstreaming electrons according their respective penetration depth into the shock front: (i) electrons which cannot penetrate the shock front before being reflected back, (ii) electrons which penetrate the overshoot region only and stay a certain time within it, and, finally, (iii) electrons which go deeply within the downstream region. The trajectory analysis of these three populations allows to evidence distinct acceleration mechanisms. The main features are represented respectively in Figures 3, 4, and 5 for each electron class. All three selected electrons are finally located within the same final upstream area as shown in Figures 3a, 4a, and 5a (around $\theta_{Bn} \approx 55°$), but acquire a substantially different final parallel energy as these leave the shock front (Figures 3f, 4f, and 5f). We named these particles "mirrored," "trapped," and "leaked," respectively.

[19] One present difficulty with the curved geometry is to compare simultaneously the electrons trajectories with the shock front location, especially in the solar wind frame where the shock front itself propagates. To resolve this difficulty, we have used a diagnostic which represents the particle location along the local shock normal direction. For so doing, at a fixed time, a line is drawn passing through the location of the particle and the center of the shock front.

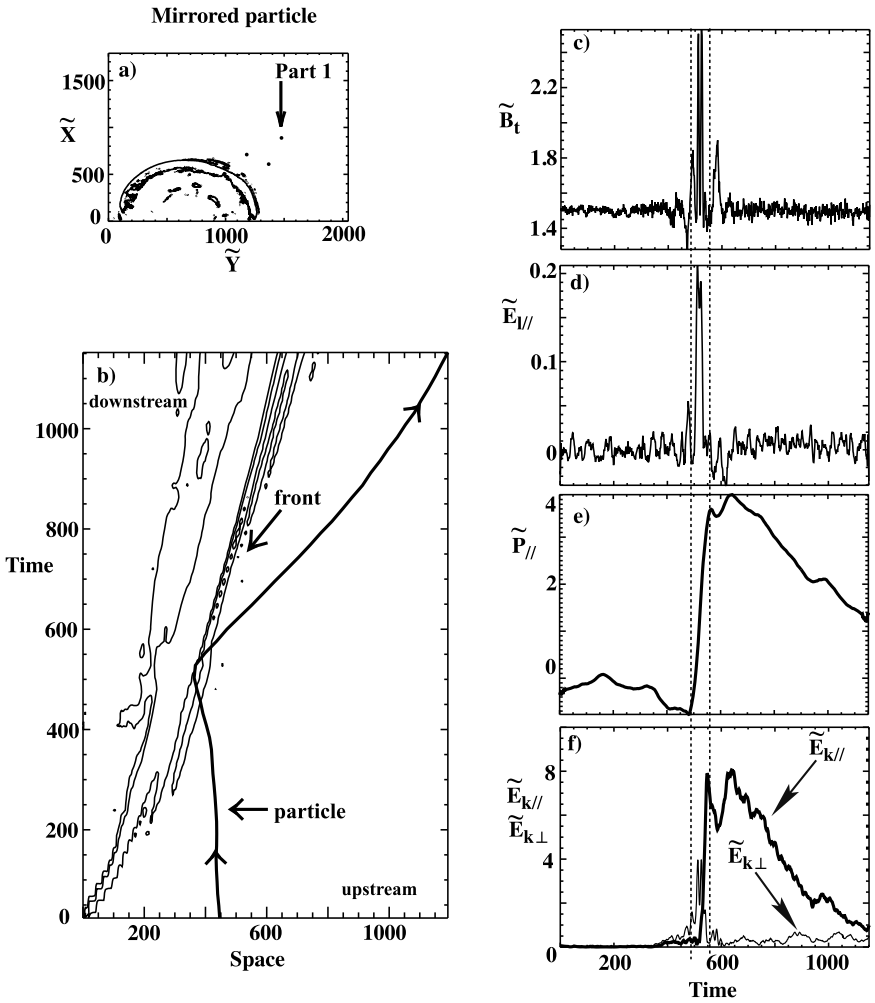

Figure 3. Individual trajectory of a backstreaming electron referenced as "mirrored" electron (particle 1). (a) The location of the three selected backstreaming electrons within the X-Y simulation plane at late time ($\widetilde{t} = 2.2\widetilde{\tau}_{ci}$); the mirrored electron is identified with an arrow. (b) The location of the selected particle along the shock front normal (thick line) with respect the location of the shock front (to see text); the main magnetic field component B_{tz} is plotted as isocontours. (c–f) The time evolution of different quantities seen by the electron: Figure 3c shows total magnetic field B_t^{total}, Figure 3d shows parallel electrostatic field component $E_{l\|}$, Figure 3e shows parallel velocity component, and Figure 3f shows parallel (solid line) and perpendicular (dashed line) kinetic energy of the particle.

This line provides the direction of the shock normal since the curved shock front has almost a circular shape. Then, the total magnetic field B_t is measured along this line. This measurement is repeated every $2\widetilde{\tau}_{ce}$ and stored in order to plot a global time stackplot as shown as Figures 3b, 4b, and 5b. The resulting composite figure allows to determine easily the relative (upstream and downstream) location of the particle with respect to the shock front along this normal direction, which is used as a reference.

3.2.1. Mirrored Particle

[20] The particle (herein particle 1) does not pass through the shock front but instead is shortly reflected back, which corresponds to a magnetic mirrored reflection type. The main interaction time range ($\Delta\widetilde{t}_{\text{int}} \approx 2.7\widetilde{\tau}_{ce}$) is defined between the dotted lines of Figure 3c, showing a large amplitude temporal spike in $\widetilde{B}_{\text{total}}$ component seen by the electron. Immediately before and after this time range, the electron suffers the influence of the small amplitude precursor (modulations in B_{total} in Figure 3c). Simultaneously, it suffers a parallel electrostatic force directed to the downstream region ($\widetilde{E}_{l\|} > 0$, see Figure 3d), but the resulting parallel acceleration is not strong enough to overcome the magnetic barrier (i.e., to fall down in the loss cone) and it is reflected back. Let us note that the electric potential jump broadens the loss cone distribution of reflected electrons and consequently tends to reduce the reflected electrons number [*Leroy and Mangeney*, 1984; *Wu*, 1984].

[21] At the same time, the kinetic energy $\widetilde{E}_k$ reported in Figure 3f shows a global increase in the parallel direction (thick line) to $\widetilde{E}_{k\|} \approx 7$ (i.e., a parallel energy gain during the reflection about $\widetilde{E}_{k\|}/\widetilde{E}_{\text{init}\|} \geq 30$), whereas the perpendicular

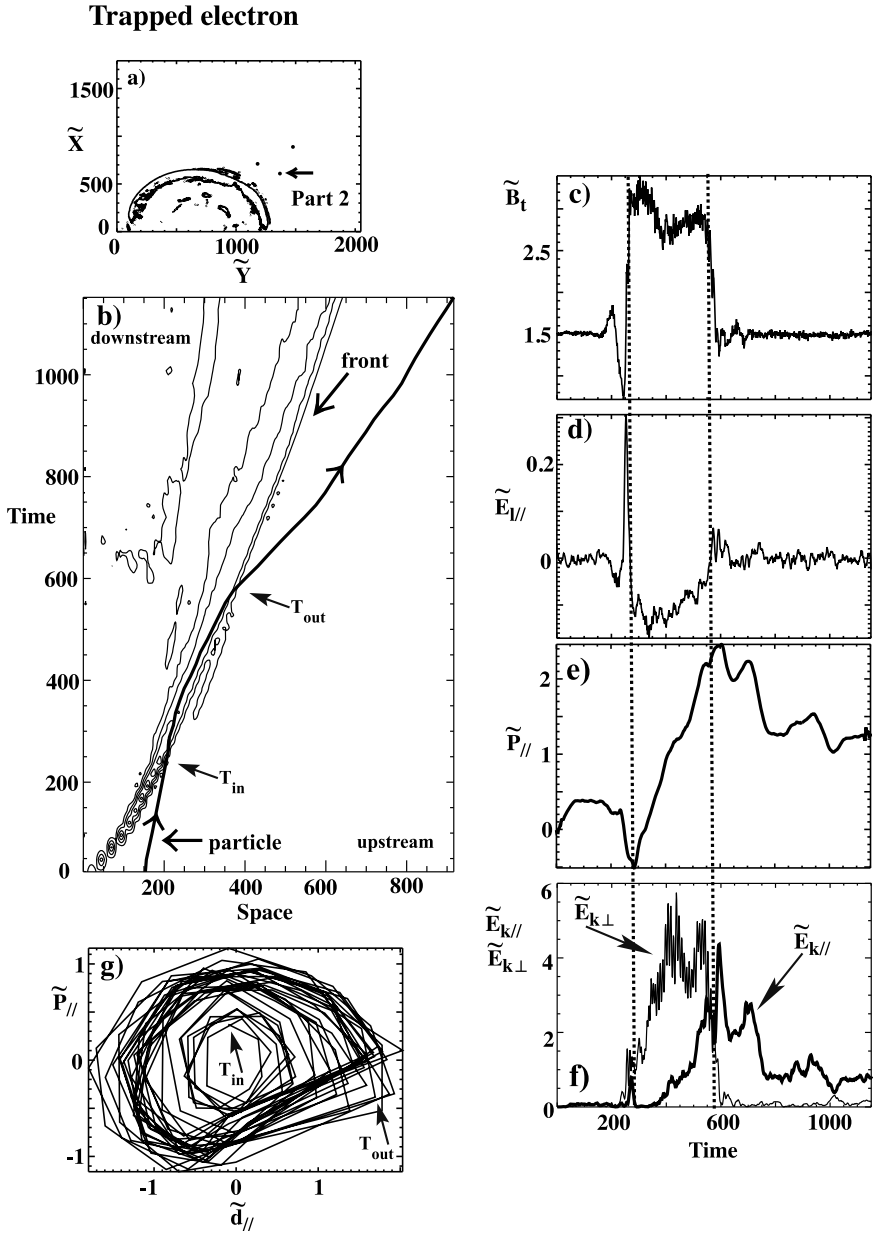

Figure 4. Same as Figure 3 for a "trapped" electron (particle 2). In addition, (g) the parallel phase space $P_{\|} - d_{\|}$ computed during the time interval $350 \geq \tilde{t} \geq 560$. This plot is obtained in the electron reference frame (bulk motion suppressed) in order to identify more precisely the trapping loop.

energy (thin line) stays almost constant (the magnetic momentum $\mu = mv^2/2B$ is conserved). All these features are retrieved for different electrons characterized by a similar and very small $\Delta\tilde{t}_{\text{int}}$. Among this class, we observe also some particles suffering very short multibounces before escaping upstream similar to those already described for a planar shock [*Lembège and Savoini*, 2002]. As a result, in a single (few) hits (fast Fermi acceleration), the particles gain enough parallel energy to escape upstream far from the shock front and populate the foreshock region.

3.2.2. Trapped Particle

[22] The selected particle (herein particle 2) succeeds in passing through the shock ramp and stays within the overshoot region (Figure 4). The magnetic field profile seen by the particle (Figure 4b) differs completely from that of Figure 3b since each particle follows a different upstream magnetic line (i.e., different local θ_{Bn} configurations) before hitting the shock front. In the present case, this electron sees a much higher amplitude electromagnetic whistler precursor than particle 1 (Figure 4c). Such differences are easily understood in terms of "time-of-flight" effects described in the literature [*Asbridge et al.*, 1968; *Filbert and Kellogg*, 1979; *Cairns*, 1987] and fully included in present simulation [see *Savoini and Lembège*, 2001]. In short, the "time-of-flight" effect is a ballistic effect due to the convection of the upstream magnetic field lines by the incoming solar wind which

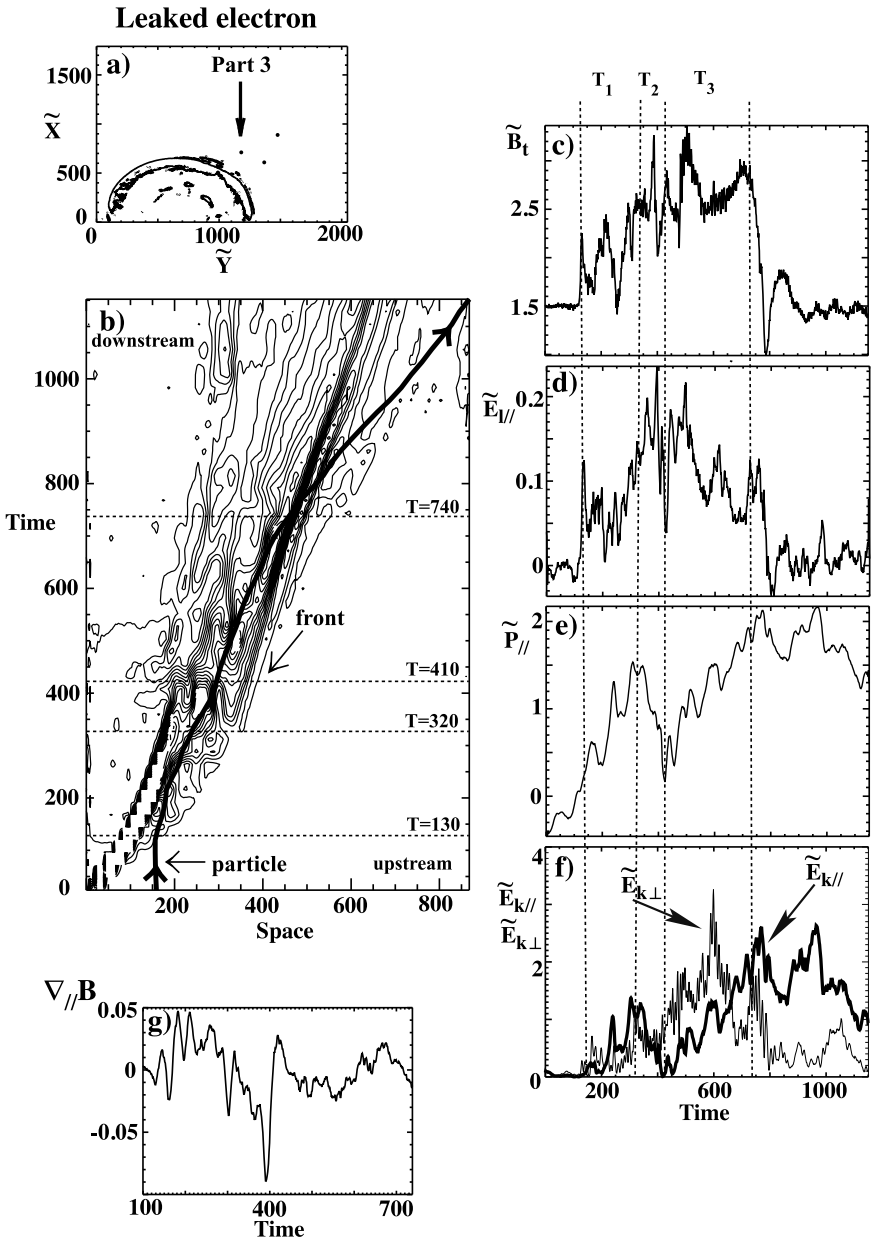

Figure 5. Same as Figure 4 for a "leaked" electron (particle 3). In addition, (g) an enlarged view of the parallel gradient of the total magnetic field $\widetilde{\nabla}_{\|}B$ computed during the time interval $510 \geq \widetilde{t} \geq 720$.

carries away the backstreaming electrons into the deeper region of the foreshock. As a result, backstreaming electrons come from different parts of the curved shock depending on their respective velocity. In the present solar wind frame, an equivalent situation is obtained since a given magnetic field line connected to the expanding curved shock scans different angles θ_{Bn} with respect to the normal of the shock front.

[23] As the electron passes through the shock ramp, it suffers a strong acceleration to $\widetilde{P}_{\|} \approx -1$ ($\widetilde{E}_{l\|}^{\max} \approx 0.3$) before being decelerated and reflected back by a negative parallel electric field ($\widetilde{E}_{l\|}^{\max} \approx -0.15$) present in the overshoot. This force is strong enough to stop the electron and to accelerate it to the shock front velocity. Then, particle 2 stays within the overshoot region for a long time (i.e., from $\widetilde{t} = 280$ to $\widetilde{t} = 550$ which represents a time interval of $\Delta\widetilde{t}_{\text{int}} \approx 40\widetilde{\tau}_{ce}^{\text{loc}}$ ($1\widetilde{\tau}_{ci}^{\text{loc}}$)), where $\widetilde{\tau}_{ci}^{\text{loc}}$ is the local ion gyroperiod (used as a reference) averaged over the transit time of the electron within the shock front. This time interval has been reported on Figures 4c, 4d, 4e, and 4f with thick vertical dotted lines within which the particle sees roughly the same amplitude of the overshoot magnetic field (≈2.8). As evidenced in Figure 4e, the parallel velocity $P_{\|}$ linearly increases during this time range.

[24] Then, the associated parallel kinetic energy increases to $\widetilde{E}_{k\|} \approx 4$ and the particle has enough energy to pass through the electric potential barrier again. After leaving the shock

front at time $\widetilde{t} = 550$, the parallel energy slightly decreases as the electron interacts with the solar wind (beam-plasma interactions). The perpendicular kinetic energy (thin line) shows a totally different behavior. It cannot be associated to the adiabatic compression since the increase of the $\widetilde{E}_{k\perp}$ is not correlated to the increase of the magnetic field which is much faster (then $\widetilde{E}_{k\perp} \neq \mu\widetilde{B}_t$). Consequently, the adiabatic invariant is not conserved ($\mu/\mu_o \approx 4$ not shown here) where μ is computed locally in the particle reference frame. Such a behavior can be observed for "demagnetized" transmitted electrons which undergo the effect of the perpendicular electrostatic field component also present in the shock front as described theoretically by *Cole* [1976] and in numerical simulations [*Lembège et al.*, 2003; *Savoini et al.*, 2005]. Moreover, the modulations observed in the parallel velocity (Figure 4e) suggest that the electron is trapped within the electrostatic field and suffers a parallel bouncing. In order to verify this scenario, an enlarged view of the phase-space diagram $\widetilde{P}_{\|} - \widetilde{d}_{\|}$ is reported in Figure 4g from $\widetilde{t} = 280$ to $\widetilde{t} = 550$, where $\widetilde{d}_{\|}$ is the spatial particle coordinate along the direction of the magnetic field projected within the simulation plane. A characteristic trapping loop is observed. This plot is obtained in the parallel reference frame of the particle where its main parallel shift in the simulation plane (bulk motion) has been removed. A local estimate of the theoretical trapping period (in normalized units) leads to $\widetilde{\tau}_{\text{bounce}} = \sqrt{2\pi\widetilde{\lambda}/|\widetilde{E}_{l\|}|} = 12.5$ (where $\widetilde{E}_{l\|}$ is the main parallel electrostatic field seen by the particle and $\widetilde{\lambda}$ the size of the potential well respectively). This value is in good agreement with the time period measured directly from the plot ($\widetilde{\tau}_{\text{measured}} \approx 11$) within the time interval $\Delta_t = 460 - 500$, where the $\widetilde{E}_{l\|}$ component is roughly constant.

3.2.3. Leaked Electron

[25] The last selected particle (herein particle 3 of Figure 5) succeeds in passing quickly through the shock front and penetrates the downstream region far behind the overshoot region. The electron stays for most of its trajectory within the downstream region ($\Delta_t \approx 2\widetilde{\tau}_{ci}^{\text{loc}}$, where $\widetilde{\tau}_{ci}^{\text{loc}}$ is the ion gyroperiod averaged over the transit time of the electron within the downstream region). One striking feature is that the electron does not see the same shock orientation θ_{Bn} as it goes into and out from the shock front. The present particle 3 originally hits the shock front in a nearly perpendicular region ($\theta_{Bn} \approx 88°$), where no reflected electrons are observed and finally succeed to escape from the downstream region in a much more oblique quasi-perpendicular domain ($\theta_{Bn} \approx 48°$), where the electrostatic barrier has a much lower amplitude (section 3.1).

[26] The dynamic of the "leaked" electrons is much more complex than that of "mirrored" or "trapped" electrons. As an example, Figure 5 plots the time history of a "leaked" electron in the same format as for the two previous classes. In Figure 5c, the magnetic field seen by the electron exhibits a characteristic almost perpendicular shock profile (with a net jump) and oblique shock profile (with large whistler precursor) as the particle respectively penetrates and leaves the front at times $t \approx 320$ and 740. Figure 5e shows the time history of the parallel electron velocity component $P_{\|}$. Three distinct time ranges indicated by vertical dashed lines may be defined: T_1 ($130 \leq \Delta\widetilde{t} \leq 320$), T_2 ($320 \leq \Delta\widetilde{t} \leq 410$), and T_3 ($410 \leq \Delta\widetilde{t} \leq 740$), when $P_{\|}$ increases, decreases, and increases again, respectively. These reference times are reported in Figure 5b and are represented by horizontal dashed lines. These indicate that the deeper excursion of the electron within the downstream region is maximum around $t \approx 320$, where the electron starts suffering some deceleration (decrease of $P_{\|}$ in Figure 5e.

[27] Within the whole time range where the electron transits within the downstream region, it suffers an overall parallel acceleration (Figure 5e) until $P_{\|}$ reaches a maximum value ($\approx$2.1) just before escaping front the shock front. However, one striking feature is that the parallel electrostatic component has not the appropriate sign (positive sign herein) to account for this acceleration and others mechanisms need to be invoked. A possible process proposed at present time is related to magnetic field fluctuations. Indeed, as is well evidenced in previous works, the downstream region is highly turbulent and is characterized by strong time and spatial magnetic field fluctuations, which is confirmed by the local B field seen by the particle (Figure 5c). Figure 5g plots the parallel magnetic field gradient $\vec{\nabla}_{\|}B$ seen by the electron as it travels behind the shock front (i.e., for $130 \leq \Delta\widetilde{t} \leq 740$). Such a gradient may evidence the magnetic bounces suffered by the electron. Indeed, for each particle bounce, the magnetic field gradient has to shows an extremum (the reflected electron goes back on the same magnetic field line) as observed in Figure 5g, and such variations are correlated with parallel acceleration in Figure 5e within time ranges T_1 and T_2. Then, the electron suffers magnetic multiple bounces (Fermi type 1) and succeeds to gain a noticeable energy.

[28] The apparent particle deceleration observed in the time range T_2 can be understood within this scenario. Indeed, no change of slope sign is observed in $\vec{\nabla}_{\|}B$ which means absence of bounces and no energy gain. Then, the deceleration imposed by the positive parallel electrostatic component $E_{l\|}$ becomes the dominant process. Moreover, let us note that, in contrast with previous electron cases, the energy gain is now shared in same proportion along the direction parallel and perpendicular to the magnetic field (Figure 5f).

4. Discussion and Conclusions

[29] The present study is an extension of a previous paper [*Savoini and Lembège*, 2001] and covers herein the whole quasi-perpendicular region of a supercritical shock ($45° \leq \theta_{Bn} \leq 90°$). It is more particularly focused on time trajectory analysis of backstreaming electrons populating the electron foreshock region. The main features of the study are based on the inclusion of (i) curvature effects, (ii) self-consistent analysis of the curved shock dynamics and full electron foreshock region (including kinetic effects and spatial/timescales of both ions and electrons), (iii) nonhomogeneities and nonstationary effects, and (iv) time-of-flight effects.

[30] Present preliminary results evidence three classes of backstreaming electrons: (i) "mirrored," (ii) "trapped," and (iii) "leaked" electrons. Although their origin and their acceleration processes are differ completely, the measurement of the penetration depth Δ_p into the shock allows to distinguish these three classes respectively by $\Delta_p \approx \widetilde{\rho}_{ce}$, $\Delta_p \geq \widetilde{\rho}_{ci}$, and $\Delta_p \gg \widetilde{\rho}_{ci}$. One can use these criteria to obtain the relative

percentage of each population, $N_{\text{mirror}} \approx 70\%$, $N_{\text{trapped}} \approx 20\%$, and $N_{\text{leaked}} \approx 10\%$. Let us note that all backstreaming electrons selected herein represent only 4.7% of the total incoming solar wind electrons. If these results are only indicative (since we use irrealistic values of the mass ratio m_e/m_i and the frequency ratio ω_{ce}/ω_{pe} because of computer constraints), these give an idea on the relative proportion of the three classes in the backstreaming population.

[31] Present results confirm quantitatively the general consensus in which backstreaming electrons are composed of magnetic-mirrored electrons. However, our results demonstrate more precisely that the oversimplified magnetic mirror process is certainly not unique. Backstreaming electrons also include electrons which are energized by nonmagnetic mirror processes as already described in previous statistical works [*Savoini and Lembège*, 2001; *Lembège and Savoini*, 2002]. Based on time trajectory analysis, we have observed the presence of nonmirrored electrons identified as "trapped" which are localized within the overshoot region and mainly suffer the effect of the parallel electrostatic field component.

[32] Moreover, we have identified a third class not previously observed, "leaked" electrons. To the knowledge of the authors, it is the first time that this electron population is identified with a self-consistent curved quasi-perpendicular shock. Contrary to the previous cases, no unique acceleration mechanism can be identified for this electron class. Complementary analysis shows that other leaked electrons may originally penetrate the front not from a certain region below 90° but rather within a wide range of oblique shock normal directions. In all cases, the trajectory is intricate and no unique acceleration process can be defined. However, it seems that all "leaked" electrons finally escape into the upstream region within an angular range below $\theta_{Bn} \approx 60°$. It appears that the escape conditions for the "leaked" electrons then require a fall down of the electrostatic barrier at the shock front (or correlated to large variation of this field) accessible only for large deviation of θ_{Bn} from 90° with our shock parameters. This field fall down plays the role of a funnel in favor of particles leakage. Such escaping conditions can explain the absence of this backstreaming population in the work by *Savoini and Lembège* [2001] which was limited to $90° \geq \theta_{Bn} \geq 65°$, where the accessibility to lower angles was not possible.

[33] Finally, the dynamic of the "leaked" electrons is much more complex than that of "mirrored" and "trapped" electrons. The acceleration mechanisms appear to change in time as the particle penetrates more or less further within the downstream region before coming back to the shock front and escaping upstream. Possible processes identified herein are multibounces within magnetic field fluctuations (particle acceleration) and/or interaction with a positive electrostatic field (particle deceleration). Complementary statistical study is necessary to clearly separate the contribution of each possible acceleration process which is beyond the scope of this paper and will be presented in an forthcoming paper.

[34] **Acknowledgments.** Simulation runs have been performed on the supercomputer center "IDRIS" located at Orsay (France). We thank Jean-Noel Leboeuf for providing the basic (periodic) version of the 2-D code.

[35] Philippa Browning thanks the reviewer for his or her assistance in evaluating this paper.

References

Anderson, K. A. (1981), Measurements of the bow shock particles far upstream from earth, *J. Geophys. Res.*, *86*(A6), 4445–4454.

Anderson, K. A., R. P. Lin, F. Martel, C. S. Lin, G. K. Parks, and H. Rème (1979), Thin sheets of energetic electrons upstream from the Earth's bow shock, *Geophys. Res. Lett.*, *6*(5), 401–404.

Asbridge, J. R., S. J. Bame, and I. B. Strong (1968), Outward flow of protons from the Earth's bow shock, *J. Geophys. Res.*, *73*(17), 5777–5782.

Bale, S., and F. Mozer (2007), Measurement of large parallel and perpendicular electric fields on electron spatial scales in the terrestrial bow shock, *Phys. Rev. Lett.*, *98*, 205001.

Bosqued, J. M., N. Lormant, J. L. Bougeret, L. Yin, M. El-Alaoui, and M. Ashour-Abdalla (1996), Simultaneous observations of electron distributions and f_pe emissions in the Earth's foreshock region by the WIND spacecraft, *Eos Trans. AGU*, *77*, 583.

Cairns, I. H. (1987), The electron distribution function upstream from the Earth's Bow shock, *J. Geophys. Res.*, *92*(A3), 2315–2327.

Cole, K. D. (1976), Effects of crossed magnetic and spatially dependent electric fields on charged particle motion, *Planet. Space Sci.*, *24*, 515–518.

Feldman, W. C., R. C. Anderson, S. J. Bame, S. P. Gary, J. T. Gosling, D. J. McComas, M. F. Thomsen, G. Paschmann, and M. M. Hoppe (1983), Electron velocity distributions near the Earth's bow shock, *J. Geophys. Res.*, *88*(A1), 96–110.

Filbert, P. C., and P. J. Kellogg (1979), Electrostatic noise at the plasma frequency beyond the Earth's bow shock, *J. Geophys. Res.*, *84*(A4), 1369–1381.

Fitzenreiter, R. J. (1995), The electron foreshock, *Adv. Space Res.*, *15*, 9–27.

Fitzenreiter, R. J., J. D. Scudder, and A. J. Klimas (1990), Three-dimensional analytical model for the spatial variation of the foreshock electron distribution function: Systematics and comparisons with ISEE observations, *J. Geophys. Res.*, *95*(A4), 4155–4173.

Fitzenreiter, R. J., A. F. Vinas, A. J. Klimas, R. P. Lepping, M. L. Kaiser, and T. G. Onsager (1996), Wind observations of the electron foreshock, *Geophys. Res. Lett.*, *23*, 1235–1238.

Kasaba, Y., H. Matsumoto, Y. Omura, and R. R. Anderson (1977), GEOTAIL observation of $2f_pe$ emission around the terrestrial electron foreshock, *Adv. Space Res.*, *20*, 699–702.

Klimas, A. J., and R. J. Fitzenreiter (1988), On the persistence of unstable bump-on-tail electron velocity distributions in the Earth's foreshock, *J. Geophys. Res.*, *93*, 9628–9648, doi:10.1029/JA093iA09p09628.

Krauss-Varban, D., and C. S. Wu (1989), Fast Fermi and gradient drift acceleration of electrons at nearly perpendicular collisionless shocks, *J. Geophys. Res.*, *94*(A11), 15,367–15,372.

Lefebvre, B., S. Schwartz, A. Fazakerley, and P. Décréau (2007), Electron dynamics and cross-shock potential at the quasi-perpendicular Earth's bow shock, *J. Geophys. Res.*, *112*, A09212, doi:10.1029/2007JA012277.

Lembège, B., and J. M. Dawson (1987), Self-consistent study of a perpendicular collisonless and nonresistive shock, *Phys. Fluids*, *30*, 1767.

Lembège, B., and P. Savoini (1992), Non-stationarity of a 2-D quasi-perpendicular supercritical collisonless shock by self-reformation, *Phys. Fluids*, *AA*, 3533.

Lembège, B., and P. Savoini (2002), Formation of reflected electron bursts by the nonstationarity and nonuniformity of a collisionless shock front, *J. Geophys. Res.*, *107*(A3), 1037, doi:10.1029/2001JA900128.

Lembège, B., P. Savoini, M. Balikhin, S. Walker, and V. Krasnoselskikh (2003), Demagnetization of transmitted electrons through a quasi-perpendicular collisionless shock, *J. Geophys. Res.*, *108*(A6), 1256, doi:10.1029/2002JA009288.

Leroy, M. M., and A. Mangeney (1984), A theory of energization of solar wind eletrons by the Earth's bow shock, *Ann. Geophys.*, *2*, 449–456.

Liewer, P. C., V. D. Decyk, J. M. Dawson, and B. Lembège (1991), Numerical studies of electron dynamics in oblique quasi-perpendicular collisionless shock waves, *J. Geophys. Res.*, *96*(A6), 9455–9465.

Mellott, M. M. (1985), Subcritical collisionless shock waves, in *Collisionless Shocks in the Heliosphere: A Tutorial Review*, *Geophys. Monogr. Ser.*, vol. 35, edited by B. Tsurutani and R. Stone, p. 131–140, AGU, Washington, D. C.

Onsager, T. G., and M. F. Thomsen (1991), The Earth's foreshock, bow shock, and magnetosheath, *Proceedings of the IUGG General Assembly, 20th, Vienna, Austria, Aug. 11–24*, *29*, 998–1007.

Savoini, P., and B. Lembège (1994), Electron dynamics in two and one dimensional oblique supercritical collisionless magnetosonic shocks, *J. Geophys. Res.*, *99*(A4), 6609–6635.

Savoini, P., and B. Lembège (2001), Two-dimensional simulations of a curved shock: Self-consistent formation of the electron foreshock, *J. Geophys. Res.*, *106*(A7), 12,975–12,992.

Savoini, P., B. Lembège, V. Krasnosselskhik, and Y. Kuramitsu (2005), Under and over-adiabatic electrons through a perpendicular collisionless shock: theory versus simulations, *Ann. Geophys.*, *23*, 3685–3698.

Tidman, D. A., and N. A. Krall (1971), *Shock Waves in Collisionless Plasmas*, Wiley, New York.

Walker, S., et al. (2004), Electric field scales at quasi-perpendicular shocks, *Ann. Geophys.*, *22*, 2291–2300.

Wu, C. S. (1984), A fast fermi process: Energetic electrons accelerated by a nearly perpendicular bow shock, *J. Geophys. Res.*, *89*(A10), 8857–8862.

Yin, L., M. Ashour-Abdalla, J. M. Bosqued, M. El-Alaoui, and J. L. Bougeret (1998), Plasma waves in the Earth's electron foreshock: 1. Time-of-flight electron distributions in a generalized Lorentzian plasma and dispersion solutions, *J. Geophys. Res.*, *103*(A12), 29,619–29,632, doi:10.1029/98JA02294.

B. Lembége, LATMOS-IPSL-UVSQ, Quartier des Garennes, 11 Boulevard d'Alembert, F-78280 Guyancourt Cedex, France. (bertrand.lembege@latmos.ipsl.fr)

P. Savoini and J. Stienlet, LPP, Ecole Polytechnique, UPMC, Route de Saclay, F-91128 Palaiseau Cedex, France. (philippe.savoini@upmc.fr; joel.stienlet@lpp-polytechnique.fr)